Original Article

The Effects of Light Guide Thickness on the Accuracy of Position Estimation, Linearity, and Uniformity Responses of Anger Camera: a Monte Carlo Study

Hamidreza Hemmati [1], Alireza Kamali-Asl [1, *], Reza Haghshenas [1]

1- Department of Radiation Medicine Engineering, Shahid Beheshti University, Tehran, Iran.

Received: 29 October 2015
Accepted: 23 February 2016

ABSTRACT

Purpose- Some practical and theoretical efforts have been made to investigate the effects of designing parameters on the performance of anger camera. In this study, the effects of light guide thickness on the accuracy of position estimation, linearity, and uniformity response of a typical gamma camera has assessed using Geant4 Monte Carlo (MC) simulation toolkit.

Methods- Three MC simulations are done using T/R values of 0, 0.5, and 1, where T is the thickness of light guide and R is the effective radius of a hexagonal photomultiplier tube. For each T/R value, the accuracy of position estimation was investigated by the analysis of the relations between the true and estimated positions of scintillation events. Also, the differential non-uniformity and average non-linearity maps have been used to assess the effect of light guide thickness on the linearity and uniformity responses, respectively.

Results- The results showed that the accuracy of position estimation depends on the depth of scintillation causing erroneous estimated positions for T/R values of 0 and 0.5. For the case T=R, that dependency was eliminated due to the enough broadening of optical photon cones and the position estimation errors were in the range of intrinsic spatial resolution of camera.

Conclusions- Lack of a proper thickness of the light guide on the gamma camera can ruin the accuracy of position estimation on the gamma camera. In addition, both linearity and uniformity responses have a strong dependency on the thickness of light guide.

Keywords:
Anger camera,
Geant4 simulation,
Light guide,
Position estimation,
Linearity and uniformity responses.

1. Introduction

Even though there are many improved variants of scintillation camera, the classical Anger camera is still used in nuclear medicine clinics world widely [1]. A typical Anger gamma camera consists of a removable collimator, a single scintillator crystal, a light guide, an array of photomultiplier tubes (PMTs), and associated electronics [2]. It is well known that the choice of collimator mainly alters the extrinsic components of the spatial resolution, and uniformity characteristics [2]. The intrinsic performance characteristics depend on more factors, including the opto-physical properties of scintillator crystal and light guide, the response function of PMTs and electronics.

Some practical and theoretical efforts have been made to investigate the effects of different parameters on the performance of an Anger camera. Anger [3], practically recommended a crystal-detector separation equal to the tube radius for a close-packed array of PMTs. Baker

Corresponding Author:
Alireza Kamali-Asl, PhD
Radiation Medicine Engineering Department, Shahid Beheshti University, Tehran, Iran.
Tel: (+98) 2129904227
Email: a_r_kamali@yahoo.com

and Scrimger [4,5] proposed a theoretical approach for designing of an optimum Anger camera. They studied parameters including the light guide thickness, the relative PMT gain, the size and spatial arrangement of the PMTs, and the signal fractions used for positioning. Their results showed that the optimum light guide thickness for the best linearity is approximately equal to the effective radius of the PMTs. It has been shown that the depth of interaction of gamma radiation in crystal has an impact on the full-width at half-maximum (FWHM) of the light spread function [5]. The effects of the response function of gamma camera on the performance characteristics and different methods of correction have been studied by other researchers [5-9]. Surveying the literature suggests that to improve the performance of Anger camera, it is necessary to know how the system parameters could affect the accuracy of the estimated positions [3, 10-14].

In this study, the effects of light guide thickness on the accuracy of position estimation, linearity and uniformity responses of a typical Anger camera were investigated in quantitative and qualitative modes.

2. Material and Methods

2.1. Geant4 Monte Carlo Simulation Toolkit

Geant4 is an open source object-oriented toolkit for Monte Carlo simulation of the passage of particles through matter [15]. Due to state-of-the-art approaches used in Geant4 for modeling of physical processes and handling complicated geometries, it is the first candidate for optimization of imaging modalities utilizing ionizing radiation, like PET (Positron Emission Tomography), SPECT (Single Photon Emission Computed Tomography), and Compton cameras [16, 17]. In addition, the ability of Geant4 in simulation of scintillation process and tracking of the produced optical photons can be used for investigating of the effect of the optical parameters on the performance of the imaging modalities employing scintillator materials [18-20].

2.2. Simulation of Gamma Camera

In this study, a gamma camera similar to the GE DST-XLi camera (GE Healthcare Technologies, Waukesha, WI, USA) was simulated using Geant4 (version 9.4.p01). The schematic drawing of the simulated geometry is shown in Figure 1.a. Also, the implemented geometry of camera is shown in Figure 1.b. Moreover, some specifications of the system are summarized in Table 1.

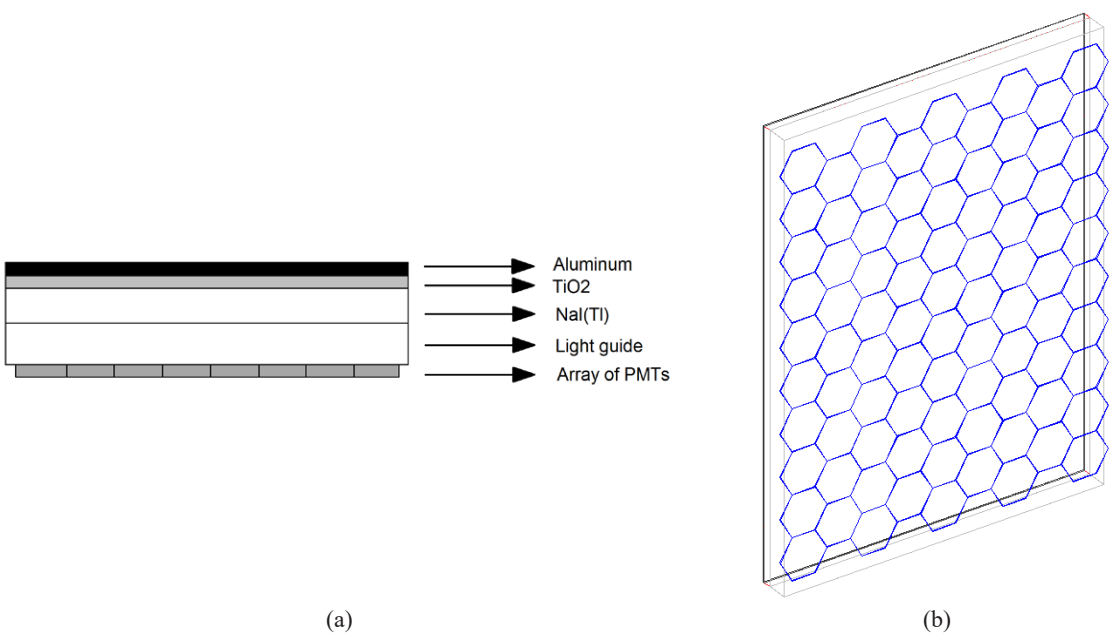

(a) (b)

Figure 1. a) Schematic drawing, and b) the 3D view of the implemented simulated gamma camera geometry.

Table 1. Specifications of Gamma camera in the simulations.

Structure levels	Material	Descriptions
First level	Aluminum	Thickness= 1 mm
Second level	TiO_2	Thickness= 1 mm thick Index of refraction= 2.69
Third level	NaI(Tl)	Shape: Planar Thickness= 9.5 mm, Area= 54 × 40 cm^2 light level yield= 3.8 × 10^4 photons/MeV
Fourth level (light guide)	Plexiglas	Thickness= 1.27 cm Index of refraction= 1.5 Area= 54 × 40 cm^2
Fifth level (PMTs)	---	Array of 86 ideal PMTs Dimension: one inch Shape: hexagonal

2.3. The Method of Assessment

2.3.1. Assessment of Position Estimation:

For each scintillation event, the energy signal was calculated by counting the number of optical photons reaching the glass surface of a PMT. The full peak energy window was set to a width of 15%. The estimated positions of scintillation events (X_S, Y_S) were calculated using equation 1:

$$(X_s, Y_s) = \left(\frac{\sum_i S_i C_{Xi}}{\sum_i S_i}, \frac{\sum_i S_i C_{Yi}}{\sum_i S_i} \right) \quad (1)$$

Where S_i and (C_{Xi}, C_{Yi}) are the counts and the center coordinates of responding PMTs, respectively. Three MC simulations were done for three camera configurations with *T/R* values of 0 (without light guide), 0.5 (with no proper thickness of the light guide), and 1 (practically based optimum thickness of light guide [3]), where *T* is the light guide thickness and *R* is the effective radius of a PMT. For each T/R values, a 12 cm-long ^{99m}Tc line source along y-axis from y= -50 mm to y= 70 mm, was imaged in the air at the distance of 10 cm from camera surface without any physical collimator. The line source was considered as unidirectional gamma rays in the simulations. The number of primaries was set to 1 × 10^6 and about scintillation events of 8 × 10^5 were recorded inside the energy window.

The effect of light guide thickness on the accuracy of position estimation was assessed using a line source as follows; for each event inside the window energy, the true position of scintillation (X_T, Y_T, z) and the estimated position using Anger logic (X_S, Y_S) is recorded. For each camera configuration, three color coded plots were drawn proportional to the depth of interaction in crystal (z), including a 3D scatter plot of the estimated positions (X_S, Y_S) versus the depth of scintillations inside the crystal, a 2D scatter plot of the estimated positions (Y_S) versus the true positions (Y_T), and a 2D scatter plot of the position estimation errors (Y_T-Y_S) versus the estimated positions (Y_S).

2.3.2. Assessment of Uniformity and Linearity Responses

The effects of light guide thickness on the linearity and uniformity responses were studied as follows: For each T/R value, a 24 cm × 24 cm ^{99m}Tc flood-field source was simulated in the air at the distance of 1 cm above the camera surface without any physical collimator. Only unidirectional gamma rays perpendicular to the surface of camera were used as primaries. The number of primaries was set to 2.5 × 10^6 and about scintillation events of 2 × 10^6 inside the energy window were recorded. Also, the true and estimated positions of scintillation events were recorded and two sets of images were acquired in 70 × 70 image matrix with a pixel size of 4 mm × 4 mm.

In this study, a novel method based on the differential non-uniformity map was used as follows to assess the effect of the light guide thickness on the uniformity response: Firstly, for

each camera configuration the acquired flood-field image was smoothed. Then, for each five consecutive pixels across all rows and columns of the smoothed image, the values of non-uniformity were calculated using equation 2.

$$\text{Nonuniformity}=\left(\frac{C_{\max}-C_{\min}}{C_{\max}+C_{\min}}\right)\times 100 \qquad (2)$$

where, C_{max} and C_{min} are the maximum and minimum pixel counts [21].

To investigate the effect of light guide thickness on the linearity response, the idea of average non-linearity map which was introduced as follows: Firstly, for all scintillation events, the pixel locations were determined using the true positions. Secondly, the value of each pixel in an empty image (with equal size to the true image) was calculated as the sum of absolute differences between the true and estimated positions of the scintillation events which fall inside the corresponding pixel of the true image. The value of each pixel was divided by the counts of the corresponding pixel in the true image plus one (to avoid zero division). It is worth noting that the values of pixels in those maps are the measures of local nonlinearities over the estimated image and are not absolute values. In addition, for each T/R values of 0, 0.5 and 1, the true image, estimated image, differential non-uniformity map and average nonlinearity map were investigated quantitatively, by the histogram analysis.

2.4. Validation of Simulation

Validation of the simulation of gamma camera was done by comparing the manufacturer reported intrinsic spatial and energy resolutions values with the calculated values from simulation (Table 2 and 3). The energy resolution was calculated by fitting a Gaussian function to the count profile in the window energy of 15%. The FWHM, and FWTM along the *x* and *y* axis were calculated by fitting two Gaussian functions to the raw data without any binning.

Because there is only a single FWHM (or FWTM) value on the manufacturer report (without mention of direction), the FWHM and FWTM comparisons was performed between the calculated values at two directions with a unidirectional FWHM and FWTM. The $FWHM_X$ and $FWTM_X$ (the components of the FWHM and FWTM along the x axis) have good agreement with the values of manufacturer report (the differences are less than 5%). However, there are significant differences among the values of $FWHM_Y$ and $FWTM_Y$ with manufacturer reported values. The differences are 34% for the FWHM and 31% for the FWTM. This disagreement may be related to the shape of PMT. Figure 2 shows one of the hexagonal PMTs of camera and its imaginary equivalent rectangle. Because the effective signal sampling element (equivalent rectangle) has a width greater than its length, it seems the density of signal sampling along the y axis is almost lower than the x axis.

Table 2. Manufacturer report for intrinsic characteristics of GE DST-XLi gamma camera.

FWHM	3.4 (mm)
FWTM	6.5 (mm)
Energy resolution	< 10 (%)

Table 3. Simulation results for intrinsic characteristics of gamma camera.

Energy resolution	$FWHM_X$	$FWTM_X$	$FWHM_Y$	$FWTM_Y$
8.15 (%)	3.48 (mm)	6.24 (mm)	4.56 (mm)	8.52 (mm)

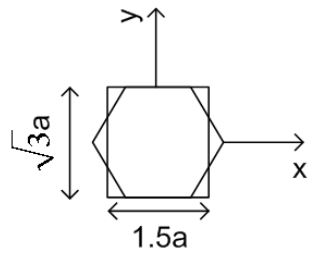

Figure 2. Drawing of one hexagonal PMT, and its equivalent rectangle. The size of hexagon side is a.

In addition, the recorded energy spectrum of the optical photons reaching the entrance windows of PMTs was compared with input light response function of NaI(Tl) scintillator in Figure 3. The root mean squared error (RSME) between two spectrums was 0.035.

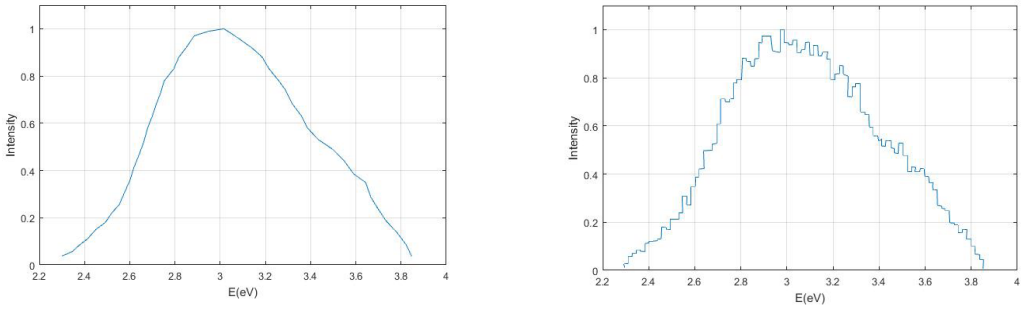

(a) (b)

Figure 3. a) The light spectrum as input data in the simulation, and b) the energy spectrum of scintillation optical photons reaching the entrance windows of PMTs.

3. Results and Discussion

3.1. Effect of Light Guide Thickness on the Accuracy of Position Estimation

3.1.1. Case T=0

Figure 4.a.1 shows that with increment of the scintillation depth, the estimated positions constrict around the centers of the responding PMTs. In this case, the scintillation photon cones broaden less than a PMT's effective diameter and equation 1 yields the center coordinates of the responding PMTs.

Figure 4.b.1 shows that the true scintillation positions can't easily be calculated from the estimated positions and the position calculation error depends on the location of scintillations (Y_T, z). So, it is not possible to recover the true positions from the estimated ones, even knowing scintillation depths. Also, Figure 4.c.1 shows that error of position estimation has a systematic complex relation with scintillations depths and estimated positions. Hence, it is not possible to assign a single range for position estimation error.

3.1.2. Case T=0.5 R

Figure 4.a.2 shows that with the increment of the scintillation depths, the estimated positions constrict around the centers of responding PMTs. Because scintillation photon cones pass through the light guide, they broaden more than the case T=0, the amount of concentration is less than the case T=0.

Figure 4.b.2 shows that for scintillation depths larger than 2 mm, the relationship between true and estimated positions is still complex and depends on the location of scintillations (Y_T, z). However, it seems there is a nearly linear relation for depths less than 1 mm. Similarly, the nonlinear fractions of signals reaching to the adjoining responding PMTs cause nonlinearities in position estimation. Finally, Figure 4.c.2 shows that the error of position estimation has a systematic complex relation with scintillations depths and estimated positions even for very shallow scintillations (depths less than 1 mm). Here again it is not possible to assign a single range for position estimation error for scintillation depths larger than 1 mm. However, there is a single range of error for scintillation depths less than 1 mm, but the relation between error and estimated positions is not linear.

3.1.3. Case T=R

The behavior of the camera with a practically based optimum thickness of light guide (T=R) is different from the two previous configurations. Figure 4.a.3 shows that the estimated positions do not constrict around any point for all scintillation depths. In this case, due to the light spreading effect of light guide, the scintillation

photon cones broaden larger than a PMT's effective diameter. Figure 4.b.3 shows that the relationship between true and estimated positions is nearly linear for all depths. So, it is possible to approximate the true positions using estimated ones. Figure 4.c.3 shows that the error of position estimation has a nearly linear relation with estimated positions. The maximum error for estimated positions is less than 5 mm. This error is in the range of intrinsic spatial resolution of a typical gamma camera. The imprecision in position estimation is mainly due to the statistical fluctuations in the number of optical photons reaching the responding PMTs.

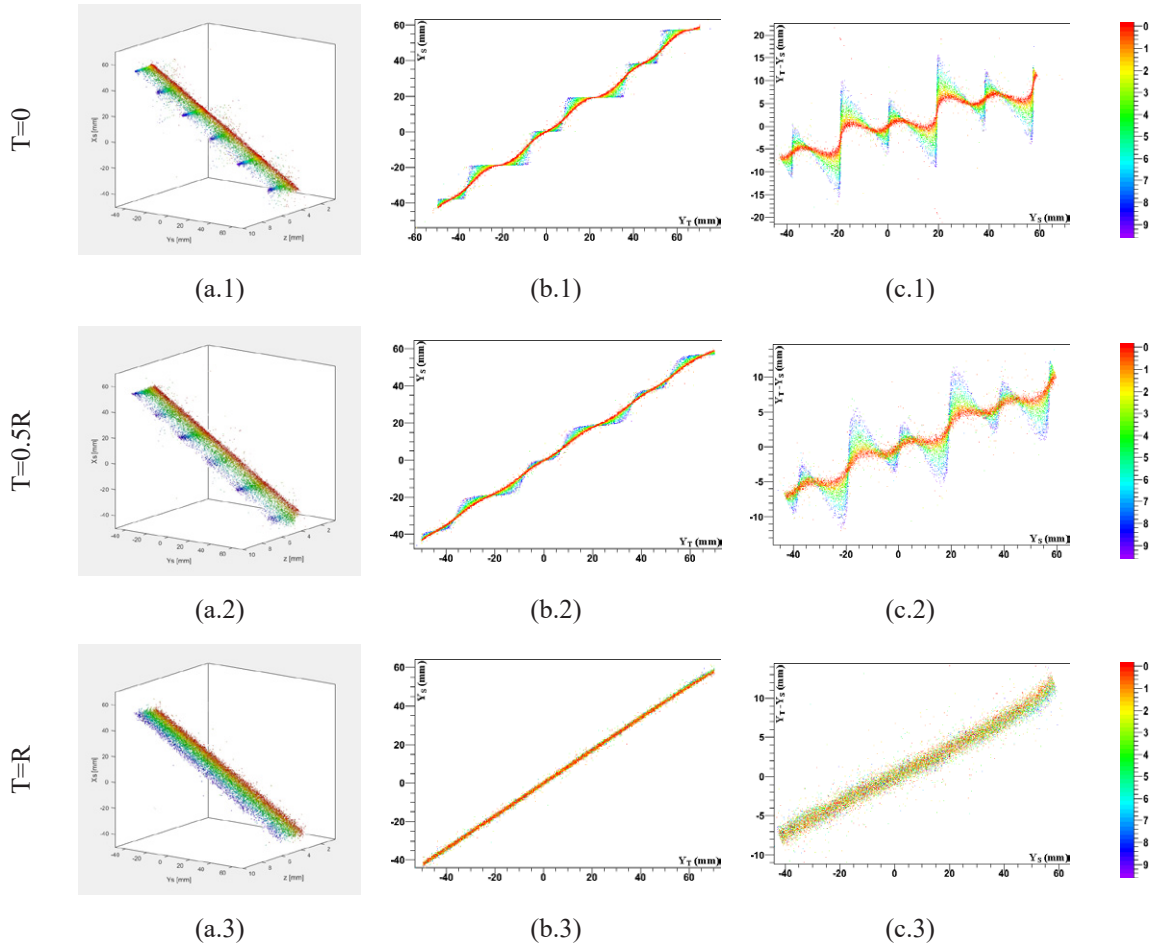

Figure 4. Color coded plots for T/R values of 0, 0.5, and 1. For each T/R value, a) 3D scatter plot of estimated positions (X_S,Y_S) versus depth of scintillations (z) inside crystal, b) 2D scatter plot of estimated positions (Y_S) versus true positions (Y_T), c) 2D scatter plot of error of position estimation (Y_T-Y_S) versus estimated positions (Y_S) and d) color bar is proportional to the depth of scintillation in the crystal (z).

3.2. The effect of Light Guide Thickness on the Uniformity and Linearity Responses of the Simulated Camera

The results of these studies are shown in Table 4 and in the first and second columns of Figure 5. The total recorded scintillation events and the average statistical error per pixel of true image are given in Table 3. The histogram of those images and maps are shown in Figures 6, and 7. Statistical mean (μ) and standard deviation (σ) of those histograms are given in Table 5.

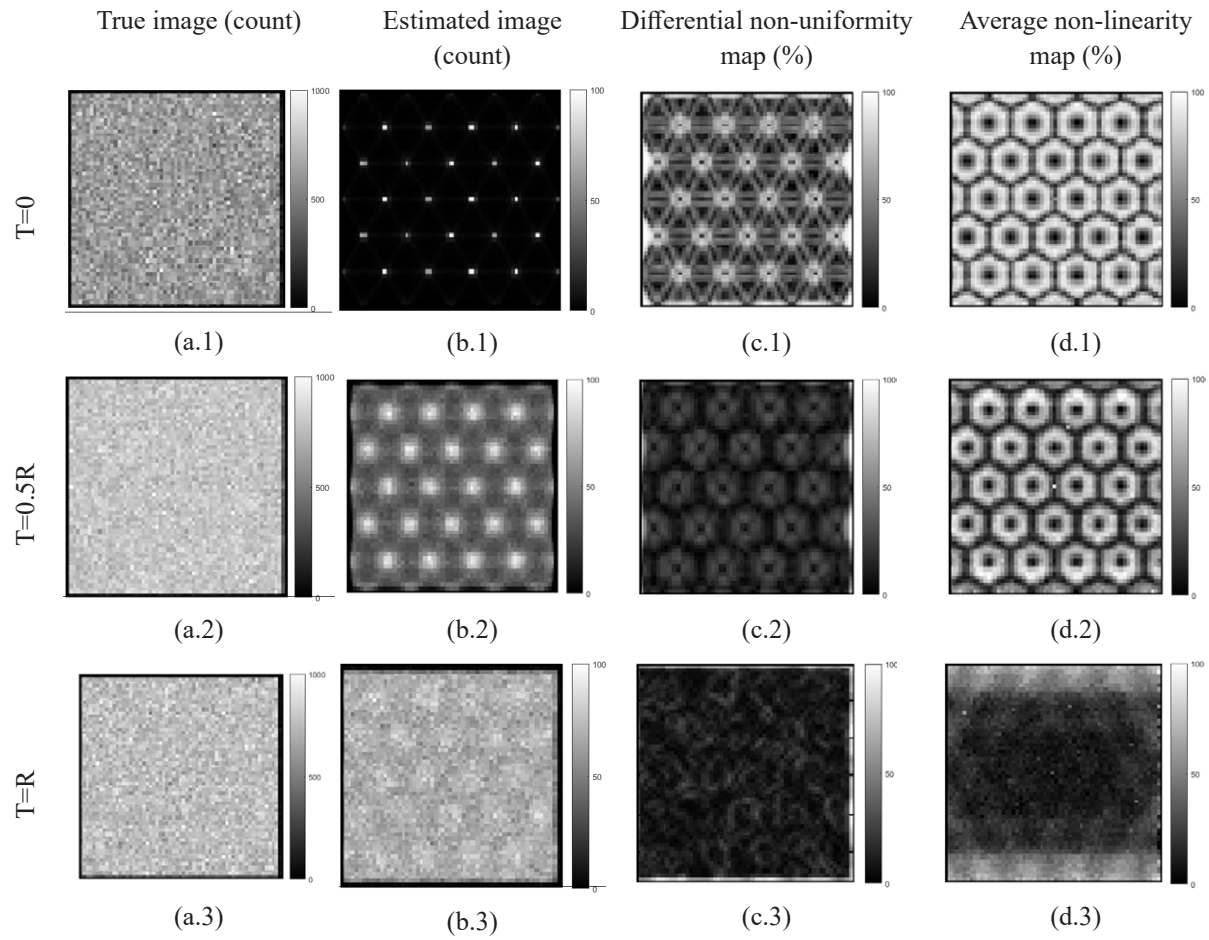

Figure 5. Responses of position estimation, non-uniformity and non-linearity to the changes of ratio of thickness of light guide to effective radius of a hexagonal PMT (*T/R*).

Table 4. Number of recorded scintillation events and average statistical error in each pixel of the true images in the flood-field source simulation.

T/R	0	0.5	1
Total recorded scintillation events	2005324	2265683	2096850
Average error in each pixel of true image (%)	4.31	4.05	4.21

Table 5. Statistical analysis of true, estimated, differential non-uniformity map and differential non-linearity map histograms, where μ and σ are mean and standard deviation, respectively.

T/R	count density of true image		count density of estimated image		differential non-uniformity map		average nonlinearity map	
	μ	σ	μ	σ	μ	σ	μ	σ
0	538.92	98.52	467.54	1335.20	43.83%	18.92%	62.90%	22.93%
0.5	608.90	94.70	579.87	236.71	12.90%	7.82%	49.52%	24.04%
1	563.52	99.54	563.32	142.75	4.63%	4.58%	26.02%	17.75%

3.2.1. Case T=0

Figure 5.b.1 shows that the output image without light guide is only an image of PMTs centers. It does not have any information about the activity distribution of the flood-field source. The histogram of that image shown in Figure 6.b.1 has a mean value of 467.54 and a standard deviation of 1335.20, respectively. Comparing this histogram

and the histogram shown in Figure 6.a.1 shows 1241% increment in standard deviation.

Figure 5.c.1 shows that there is a systematic non-uniformity over the estimated image. Histogram of this map is shown in Figure 7.a.1. This histogram shows that differential non-uniformity extends from 5% to 100% with a mean value of 43.83% and a standard deviation of 18.92%. The pattern of this map could be categorized into several areas, including dark pixels at the center of PMTs, light pixels at the circular areas around PMTs, dark connecting lines between the center of PMTs, dark triangular areas, white marginal lines between triangular area and dark lines and white areas near the left and right sides of the whole map. The latter one shows non-uniformity larger than 90%. The dark triangular areas have small non-uniformities up to 20%. The latter has very low count levels inside the estimated image (less than 500). Locations exactly at the center of PMTs and around them show considerable non-uniformities (larger than 40%). Dark connecting lines have considerable non-uniformities (up to 25%). White circular areas have non-uniformities larger than 60%. That ghastly non-uniformity map is the result of great differences in count levels of adjoining pixels of estimated image (shown in 5.b.1). The reason is the inaccuracy of position estimation due to the absence of light guide (Figures 4.a.1, 4.b.1, and 4.c.1).

Figure 5.d.1 shows that there is also a systematic average non-linearity over the estimated image. The histogram of this map (Figure 7.a.1) shows that the average non-linearity extends from 0% to 100% with a mean value of 62.90% and a standard deviation of 22.93%. The pattern in Figure 5.d.1 can be categorized into three areas including dark circular areas around the center of PMTs, white peripheral areas around them, and dark honeycomb area. The low average non-linearity of latter (less than 35%) is the result of symmetry in the gamma camera structure. All scintillation photon cones originating from these symmetric areas could stimulate signals in more than one PMT and that guarantees the accuracy of position estimation. The white areas around the center of PMTs have high average nonlinearity (larger than 70%). The reason is that scintillation photon cones originating from those areas except for very shallow scintillations, reach to only one PMT and as explained above (see Figure 4.a.1) the estimated positions constrict around the centers of responding PMTs. However, for very shallow scintillations, photon cones originating from those areas broaden enough to stimulate signals in more than one PMT and as explained above (see Figure 4.c.1) nonlinear fractions of signals cause inaccurate position estimation with large average non-linearity. The dark shaded circular areas at the center of PMTs have various average nonlinearity values from 1% at the center to 46% at peripheries. For scintillations originating from the locations exactly on the top of PMT's centers, position estimation is always accurate due to the absence of light guide. For very shallow scintillations, originating from the locations not very far from the center of PMTs, the position estimation is inaccurate and the error of position estimation is very small (about 1 mm for red curve as shown in Figure 4.c.1).

3.2.2. Case T=0.5 R

Figure 5.b.2 shows that the output image of gamma camera with no proper thickness of light guide (T=0.5R) which is severely dominated by PMTs' pattern and still has no reliable information about the activity distribution of the flood-field source. Comparing the histogram of this image and the histogram of true image shown in Figure 6.a.1 shows 149.95% increased standard deviation. It reveals that in this case, the gamma camera could seriously degrade the input information.

Besides, Figure 5.c.2 shows that there is a systematic non-uniformity over the estimated image. A comparison of Figure 5.c.2 with Figure 5.c.1 indicates that the maximum non-uniformity decreased from 100% to 66% at boundaries of the image. The pattern of this map shows a dark honeycomb with non-uniformity values up to 10%, dark lines connecting the center of PMTs with non-uniformity values between 10% and 15%, and light areas inside PMTs with non-uniformity values from 15% at peripheries to 25% toward the centers. Such a rigorous non-uniformity pattern is due to the count differences between the adjoining pixels in the estimated image (shown in 5.b.2). The inaccuracy of position estimation due to non-linear fractions of responding PMTs signals seems

to be the reason (as discussed in Figures 4.a.2, 4.b.2, and 4.c.2).

Figure 5.d.2 shows a systematic average non-linearity over the estimated image shown in Figure 5.b.2. This histogram (Figure 7.a.1) shows that the average non-linearity extends from 0% to 100% with a mean value of 49.52% and a standard deviation of 24.04%. This pattern is very similar to Figure 5.d.1 but its honeycomb area is a little thicker than the honeycomb area Figure 5.d.1. Comparing histograms in Figure 7.b.1 and 7.b.2 shows a considerable equalization over the average non-linearity values.

3.2.3. Case T=R

In contrast to the two previous cases, Figure 5.b.3 shows that the output image of gamma camera with the optimum light guide thickness ($T=R$) is a tolerable estimation of flood-field source. However, PMT pattern is still visible. A comparison of Figure 5.c.3 with Figure 5.c.2 indicates that maximum non-uniformity considerably decreased from 66% to 30% at boundaries of estimated image (shown in Figure 5.b.3). The distorted non-uniformity pattern shows random dark and light areas. Its histogram (Figure 7.a.3) has a mean value of 4.63% and a standard deviation of 4.58%. However, there is a significant reduction in these values compared to other cases (T=0 and T=0.5R cases), but the lighter areas still have considerable amount of non-uniformity (up to 10%). The reason is that the average count level in the estimated image is very low due to the small number of primaries and statistical noise being larger than the acceptable range.

Figure 5.d.3 shows that there is still a systematic average non-linearity over the estimated image. Comparing its histogram and other histograms shown in Figure 7.b.1 shows a considerable improvement in the uniformity response of camera (due to the effect of light guide). However, the large amount of non-linearity at the top and the bottom of this image suggests that the useful field of view of camera does not have to be chosen as the rectangle connecting the center of outer responding PMTs. A reason may be that the spatial arrangement of PMTs along x and y axis is not the same.

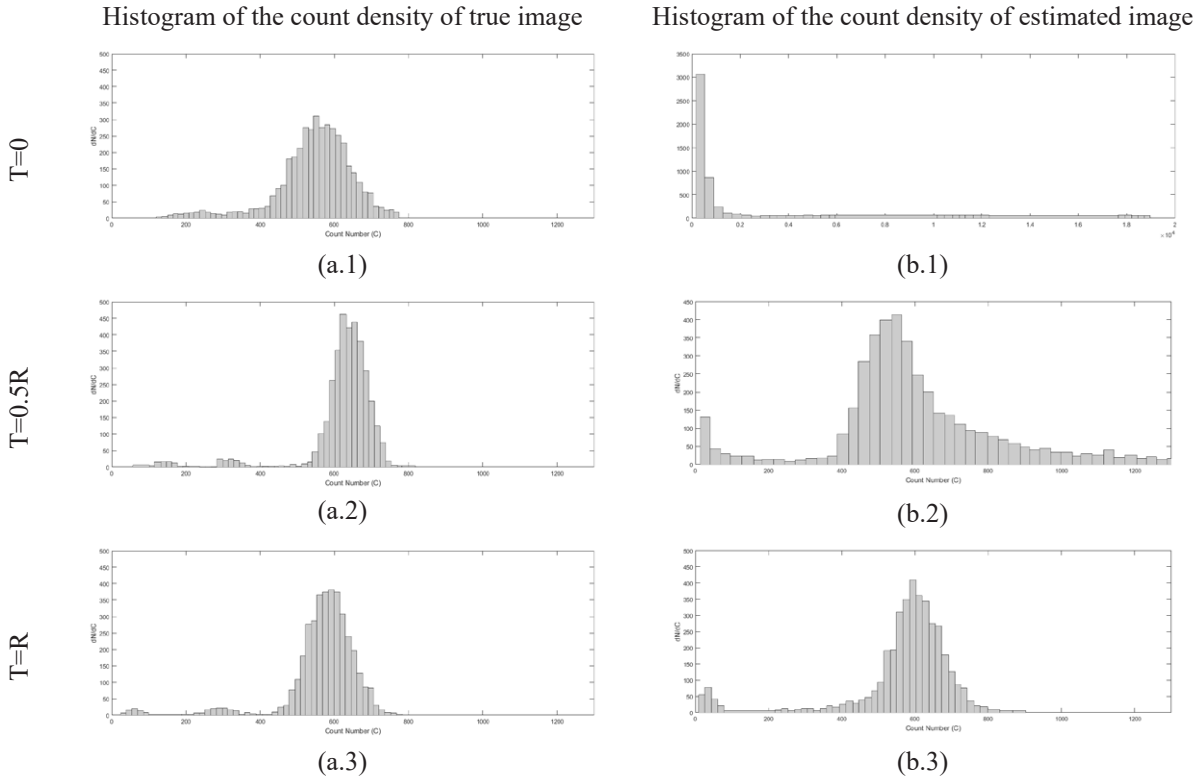

Figure 6. a) The histogram analysis of the true and b) estimated images to the rate of light guide thickness to the effective radius of a PMT.

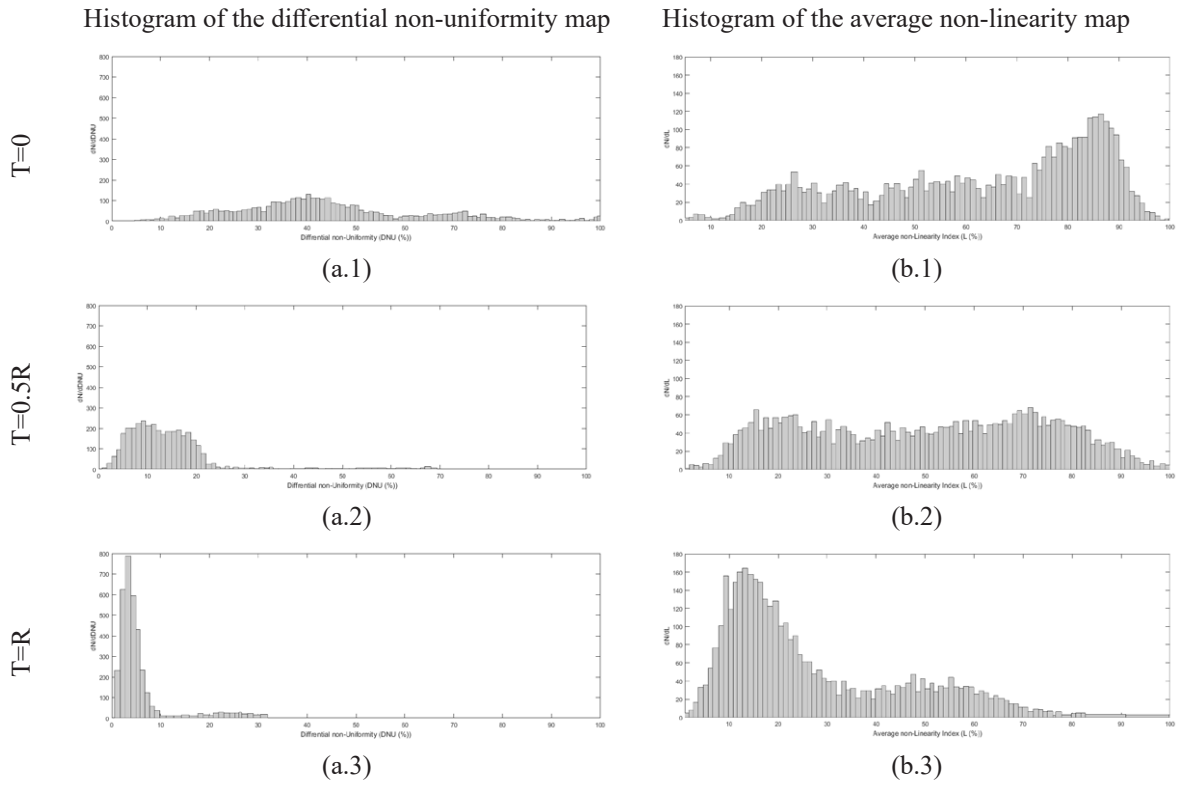

Figure 7. a) The histogram analysis of differential non-uniformity and b) non-linearity at the different rate of light guide thickness to the effective radius of a PMT.

It seems that the improvement of non-linearity response of the gamma camera with optimum light guide thickness has an intrinsic limit even using ideal PMTs. Due to the inverse-square law ($1/r^2$) and different depth of scintillation for each event, the cones of optical photons reaching the PMTs have non-uniform distribution. As a result, it is suggested to use conventional Anger logic for position estimation which encounters a biased estimation. The non-uniform distribution of optical photons results in nonlinear fractions of signals in adjoining responding PMTs.

Depending on the shape of the scintillation crystal, practical constraints and geometry considerations, a certain surface treatment of light guide and PMT are required to obtain a large light output, good uniformity and energy resolution. Recently, an application of rectangular PMTs instead of the hexagonal shape of PMTs is performed by some developers. However, in general it is advisable to choose the diameter of the light guide slightly smaller than the diameter of the PMT since the outer area of a PMT is often less sensitive that the center. But the light guide thickness has a significant impact on the uniformity and spatial resolution of system; hence it needs further investigations.

4. Conclusion

In this work, the effects of light guide thickness on the accuracy of position estimation, linearity and uniformity responses of a typical Anger camera were investigated using Geant4 Monte Carlo simulation toolkit, qualitatively and quantitatively. The results indicate that the lack of a proper thickness of the light guide, different amount of light sharing among responding PMTs - due to the depth of scintillation events - could ruin the accuracy of position esimation and encounters erroneous results. It is also shown that the uniformity and linearity responses of simulated Anger camera depend strongly on the light guide thickness. In the optimum light guide thickness, for all scintillation depths, the relationship between true and estimated positions is nearly linear due to the enough broadening of scintillation photon cones across the adjoining responding PMTs. In this case, the error of position estimation has

a linear relation with estimated positions with maximum value less than 5 mm, which is in the range of intrinsic spatial resolution of the simulated camera.

It was also shown that in the case of optimum light guide thickness, imaging a flood field source produces a tolerable uniform image. Finally, it has been noticed that the useful field of view of the camera with optimum thickness of light guide has to be chosen carefully to avoid large non-linearity observed over the boundaries of output image.

References

1- T. E. Peterson, and L. R. Furenlid, "SPECT detectors: the Anger Camera and beyond," *Physics in medicine and biology*, vol. 56, no. 17, pp. R145, 2011.

2- J. T. Bushberg, and J. M. Boone, The essential physics of medical imaging: Lippincott Williams & Wilkins, 2011.

3- H. O. Anger, "Scintillation camera," *Review of scientific instruments*, vol. 29, no. 1, pp. 27-33, 1958.

4- R. Baker, and J. Scrimger, "An investigation of the parameters in scintillation camera design," *Physics in medicine and biology*, vol. 12, no. 1, pp. 51, 1967.

5- J. Scrimger, and R. Baker, "Investigation of light distribution from scintillations in a gamma camera crystal," *Physics in medicine and biology*, vol. 12, no. 1, pp. 101, 1967.

6- J. Bradshaw, C. Burnham, J. Correia, W. L. Rogers, and N. Clinthorne, "Application of Monte-Carlo methods to the design of SPECT detector systems," *Nuclear Science, IEEE Transactions on*, vol. 32, no. 1, pp. 753-757, 1985.

7- J. Joung, R. S. Miyaoka, S. Kohlmyer, and T. K. Lewellen, "Implementation of ML based positioning algorithms for scintillation cameras," *Nuclear Science*, *IEEE Transactions on*, vol. 47, no. 3, pp. 1104-1111, 2000.

8- J. Joung, R. Miyaoka, S. Kohlmyer, and T. Lewellen, "Investigation of bias free positioning estimators the scintillation camera." pp. 20/25-20/28 vol. 3.

9- J. Vesel, and M. Petrillo, "Improved gamma camera performance using event positioning method based on distance dependent weighting." pp. 2445-2448.

10- E. Tanaka, T. Hiramoto, and N. Nohara, "Scintillation cameras based on new position arithmetics," *Journal of Nuclear Medicine*, vol. 11, no. 9, pp. 542-547, 1970.

11- H. O. Anger, "Sensitivity, resolution, and linearity of the scintillation camera," *Nuclear Science*, IEEE Transactions on, vol. 13, no. 3, pp. 380-392, 1966.

12- A. Hughes, and P. Sharp, "Factors affecting gamma-camera non-uniformity," *Physics in Medicine and Biology*, vol. 33, no. 2, pp. 259, 1988.

13- N. Royle, R. Speller, "The effects of collimation on image formation in Anger gamma cameras", Nuclear Science Symposium and Medical Imaging Conference, 1994 IEEE Conference Record; 1994.

14- H. D. Royal, P. H. Brown, and B. C. Claunch, "Effects of a reduction in crystal thickness on Anger-camera performance," *Journal of nuclear medicine*: official publication, Society of Nuclear Medicine, vol. 20, no. 9, pp. 977-980, 1979.

15- S. Agostinelli, J. Allison, K. a. Amako, J. Apostolakis, H. Araujo, P. Arce, M. Asai, D. Axen, S. Banerjee, and G. Barrand, "GEANT4—a simulation toolkit," Nuclear instruments and methods in physics research section A: Accelerators, Spectrometers, *Detectors and Associated Equipment*, vol. 506, no. 3, pp. 250-303, 2003.

16- P. Arce, J. I. Lagares, L. Harkness, L. Desorgher, G. de Lorenzo, Y. Abreu, and Z. Wang, "GAMOS: An easy and flexible way to use GEANT4", Nuclear Science Symposium and Medical Imaging Conference (NSS/MIC), IEEE; 2011.

17- S. Jan, G. Santin, D. Strul, S. Staelens, K. Assie, D. Autret, S. Avner, R. Barbier, M. Bardies, and P. Bloomfield, "GATE: a simulation toolkit for PET and SPECT," *Physics in medicine and biology*, vol. 49, no. 19, pp. 4543, 2004.

18- M. Janecek, and W. W. Moses, "Simulating scintillator light collection using measured optical reflectance," *Nuclear Science*, *IEEE Transactions on*, vol. 57, no. 3, pp. 964-970, 2010.

19- D. J. van der Laan, D. R. Schaart, M. C. Maas, F. J. Beekman, P. Bruyndonckx, and C. W. van Eijk, "Optical simulation of monolithic scintillator detectors using GATE/GEANT4," *Physics in medicine and biology*, vol. 55, no. 6, pp. 1659, 2010.

20- F. R. Rannou, V. Kohli, D. L. Prout, and A. F. Chatziioannou, "Investigation of OPET performance using GATE, a Geant4-based simulation software," *Nuclear Science*, *IEEE Transactions on*, vol. 51, no.

5, pp. 2713-2717, 2004.

21- G. F. Knoll, Radiation detection and measurement: John Wiley & Sons, 2010.

22- S. R. Cherry, J. A. Sorenson, and M. E. Phelps, *Physics in nuclear medicine*: Elsevier Health Sciences, 2012.

23- J. T. Bushberg, and J. M. Boone, The essential physics of medical imaging: Lippincott Williams & Wilkins, 2011.